JOURNAL OF MATERIALS SCIENCE 17 (1982) 925–935

Review
Studies on dechannelling by defects and on lattice site location of hydrogen in face-centred cubic metals

J. MORY
Section d'Etude des Solides Irradiés, C.E.N. B.P.6, 92260 Fontenay-Aux-Roses, France

E. LIGEON
Département de Recherche Fondamentale, C.E.N. 85X, 38041 Grenoble Cedex, France

Positive heavy particles (protons, α-particles, etc.) which propagate in a crystal lattice parallel or almost parallel with a dense axis or plane will be constrained to move along this direction for long distances owing to steering collisions with the atoms constituting the channel walls. Their relatively stable oscillating trajectories follow a potential valley described by low electronic charge density. These particles have longer paths than those propagating in an arbitrary direction ("random trajectory") and are said to be channelled. As this phenomena has many important applications, the main theoretical and experimental results obtained in two laboratories of the Commissariat à l'Energie Atomique (CEA) concerning the effect of crystal defects on channelling and the utilization of channelling to determine the lattice location of hydrogen in face-centred cubic crystals are given herein.

1. Study of dechannelling by crystal defects

It is clear that the "ease" of channelling is related to crystal perfection. It is also clear that anything which destroys this perfection, phonons, defects, etc., must change the channelling. On the other hand, the character of the channelling obviously allows one, in principle, to say something regarding the defects.

This simple idea is used both to theoretically evaluate the dechannelling effects of crystal imperfections and to observe them experimentally

1.1. Theoretical models of dechannelling by defects

The dechannelling by defects is described here by classical mechanics for particles of mass either equal to or higher than that of the proton.

When a channelled particle approaches a defect, its trajectory is more or less altered. Specifically, its total transverse energy, $E_\perp$, is modified, and the calculation of the dechannelling coefficient is equivalently that of estimating the probability that $E_\perp$ be greater than a critical transverse energy, $E_{\perp c}$. $E_{\perp c}$ depends only on the crystal and on the particle and can be evaluated by means of the Lindhard theory of channelling (see Fig. 1) [1].

Continuing with the present idea, the dechannelling coefficient can be expressed by a probability, a characteristic scattering length ("dechannelling width") or a cross-section which are dependent both on defect characteristics (nature, size) and on those of the particle (charge, energy).

A defect will cause dechannelling by both obstructing and deforming the channel containing the particle. Fortunately, in most cases, defects can be divided into two categories: those defects that dechannel mainly by means of obstruction (interstitials, stacking-faults, gas bubbles, voids and anti-phase boundaries), and those defects (disloca-

0022–2461/82/040925–11$03.82/0

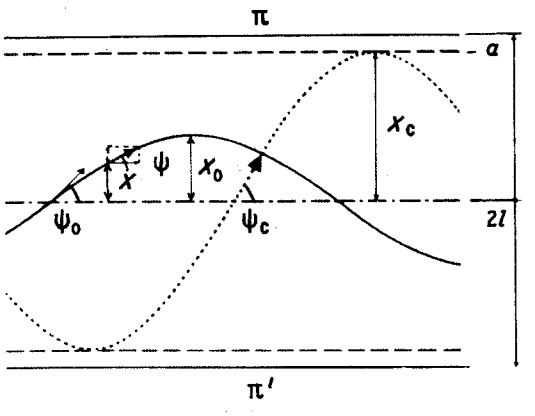

Figure 1 Principle of planar channelling. Solid line: a channelled particle of energy, E, oscillates between the planes ($\pi\pi^{-1}$) with an amplitude, X_0; the maximum angle of its trajectory with the median plane is Ψ_0. At any given time, its elongation is X, its current angle is Ψ and its total transverse energy is $E_\perp = E\Psi^2 + V(X) = E\Psi_0^2 = V(X_0)$. Dotted line: the maximum amplitude X_c, is equal to $X_c = l - a$ (where $2l$ is the interplanar distance and a the minimum particle–plane approach distance) and the maximum angle with the median plane is Ψ_c. The critical total transverse energy, $E_{\perp c}$, is $E_{\perp c} = E\Psi_c^2 = V(x_c)$. l, a, and the length of oscillation are of the order of 0.1, 0.01 and 100 nm, respectively. For better clarity, the ordinates have been multiplied by a factor about 100 with respect to the abscissae.

tions, Guinier–Preston zones) that perturb particle trejectories principally by the channel deformation they cause. Dechannelling by thermal agitation is a particular case which will be treated separately.

Unless otherwise stated, the numerical values given will be based on 5 MeV α-particles propagating between high-density planes (that is, {1 1 1} planes in f c c and {1 1 0} planes in b c c).

1.1.1. Interstitial atoms

Interstitial atoms [2–4], not occupying normal lattice sites, obviously obstruct certain channels. In such channels, the variation of $E_\perp$ is described by Rutherford scattering, and the dechannelling probability is thus expressed by a cross-section, σ_d. The complete calculation of σ_d shows that it varies as $E^{-1/2}$, and that it is relatively independent of the atomic number of the interstitial, while being relatively sensitive to the screening of the nucleus by the electron cloud (degree of ionization). For instance, σ_d is found to be about the same for hydrogen and carbon ($\sigma_d \simeq 5.10^{-5}$ nm^2 between {1 1 1} planes in palladium).

1.1.2. Stacking faults

A stacking fault [3, 5, 6] causes a shift of the crystallographic axes and planes in its immediate vicinity. Equivalently, it shifts the potential valleys (see Fig. 2) and thus gives rise to a local variation of $E_\perp$. This variation or change in $E_\perp$, $\Delta E_\perp$, can be either positive or negative depending on the transverse position ("phase") of the particle in the channel when it encounters the defect (in this case, the stacking fault). The calculation of the dechannelling probability thus involves the calculation of the probability that the transverse position of the particle in the channel falls inside a critical region (Δx in Fig. 2) defined by $E_\perp + \Delta E_\perp \geqslant E_{\perp c}$. For example, we obtain energy-independent probabilities of the order of 0.2 (in gold) or 0.3 (in aluminium).

1.1.3 Gas bubbles

The gas constituting the bubbles [7] plays a negligible role in the dechannelling process. The dechannelling probability, χ, of a gas bubble is thus simply related to the probability that a particle not be rechannelled on re-entering the crystal after traversing the gas bubble. The calculation is about the same as for the stacking fault. If one assumes that the planes are not deformed near the surface of the hole, it can be shown that χ varies linearly with the diameter and that it follows an $E^{-1/2}$ law

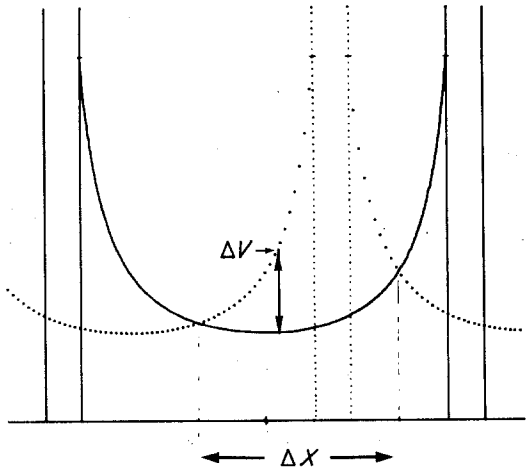

Figure 2 Stacking fault in a crystal in terms of particle–atomic plane potential. Successive potential valleys in which the channelled particles move are suddenly shifted by the stacking fault. When they cross the defect, the particles suffer a variation of their total transverse energy ($\Delta E_\perp = \Delta V > 0$, in the region denoted ΔX).

for small holes (diameter $\leqslant 10$ nm). χ reaches a limiting value, χ_{max} (in aluminium, $\chi_{max} \simeq 0.25$) independent of the energy for large diameters ($\geqslant 100$ nm).

1.1.4. Dislocations

Dislocations [6, 8–12] bend the channels, and thus the channelled particles suffer a centrifugal force which modifies their transverse energy. The calculation of the dechannelling probability in this case leads to a cross-section per unit length, λ, (that is, to a dechannelling width) given by $\lambda = k(bE)^{1/2}$, where b is the Burger's vector, E is the kinetic energy of the particle and k is a constant which depends on the nature of the crystal, the particle and the dislocation (screw or edge). For example, in aluminium, we find that $\lambda \sim 17$ nm. The evaluation of λ for dislocation loops is much more complicated. According to the theory of elasticity, λ for a dislocation loop must have a value much lower than that of a straight dislocation and the value must be proportional to the diameter of the loop.

1.1.5. Guinier–Preston zones

Guinier–Preston (GP) zones [7] have, in general, different geometrical shapes: flat discs, one-atom width in thickness and about 5 nm in diameter are obtained under certain ageing conditions in Al–Cu dilute alloys. They dechannel in approximately the same way as dislocation loops, owing to the lattice deformation induced by the difference between the atomic volumes of aluminium and copper atoms. The calculation of the dechannelling coefficient is difficult, consequently, can only be given semi-quantitatively. Nevertheless, it can be postulated that GP zones dechannel much more than individual atoms, and, the greater their size, the higher their dechannelling width, λ_d.

1.1.6. Ordered alloys

Channelling conditions in ordered alloys [13] are somewhat unusual. All the planes of an {hkl} family have the same composition in the disordered phase, whereas this is obviously not the case in the ordered state. In AuCu and $AuCu_3$ ordered alloys, for instance, all the {111} planes are identical, but some of the {110} and {100} planes are alternatively enriched in either gold or copper. There is thus a dissymmetry in the planar potential which, paradoxically, leads to a higher dechannelling coefficient than that associated with the disordered state. In AuCu and $AuCu_3$ ordered alloys, for anti-phase boundaries which act somewhat like stacking faults (see Fig. 3). No calculation of the dechannelling coefficient has yet been effected.

1.1.7. Thermal agitation

Even in a defect-free crystal, a channelled beam of particles is progressively dechannelled by atoms which are no longer at their perfect crystal sites due to thermal agitation [14], and by the multiple scattering due to electrons. The main influence of thermal agitation is to thicken the planes and rows of the crystal, as the temperature increases. This induced variation in the potential can be calculated. When the temperature increases, the slope of the potential decreases and the particles are thus less constrained and undergo greater dechannelling compared to that at lower temperatures (see Fig. 4).

1.1.8. Influence of defects on energy loss

It could be expected that the energy-loss of channelled particles should be affected by the presence of defects in the crystal. In fact, it is theoretically demonstrated that this effect is quite negligible, at least in the cases of dislocations [15] and hydrogen interstitials [16]. For instance, the energy-loss of channelled α-particles increases by about 0.1 per cent when a sample of palladium contains a concentration of 1 per cent of hydrogen interstitials. Experimentally, no change has been observed in the maximum energy of protons transmitted through tantalum samples either containing or not containing dislocations [17].

1.2. Experimental evidence

A simple technique has been developed which consists of bombarding polycrystals or single crystals

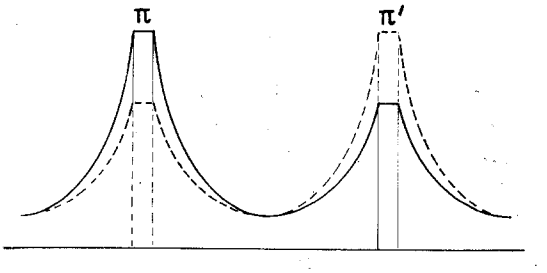

Figure 3 The trajectory of channelled particles moving between {100} planes in an ordered alloy of $AuCu^3$ structure is governed by a dissymmetrical potential. Moreover, this dissymmetry is periodically reversed by anti-phase boundaries.

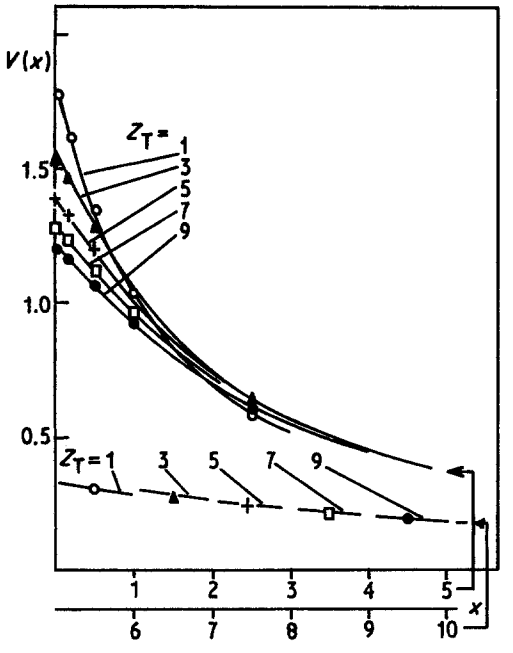

Figure 4 Calculated variation of the planar channelling as a function of the thermal agitation. Z_T is a parameter which varies as the mean quadratic displacement of the atoms. X is the particle–plane distance, in Thomas–Fermi radius units.

with a beam of positive mono-energetic particles. The thickness of the sample is chosen so that only channelled particles (whose range is greater than that of random particles) emerge, the emerging beam being made up of many sub-beams parallel to the main directions of the crystal.

The particles are either collected in a counter or registered on a film. In the latter case, one obtains an image called a "channellograph", whose constrast is related to the local orientation and imperfections of the crystal.

The particles can be either obtained from a radioactive source or from an accelerator. In the first case, excellent flux and energy stability is obtained and quantitative experiments are easily performed. In the second case, there is obviously a wider choice of particles and energies. Fig. 5 indicates the principle of an experiment conducted with a radioactive source [8].

If a small diaphragm is inserted just behind the crystal, the channelled particles emerge parallel to dense planes and axes ("channellographic projection") (see Fig. 6). Then, at the detector (film), a pattern is observed which is the result of the intersection of the direct lattice and the detector (see Fig. 7). In particular, this pattern allows determination of the orientation of the crystal [19].

The situation is approximately the same when the radiation protection of the source contains pin-holes. In the immediate vicinity of the pin-holes covering a particular grain, patterns are observed on the channellograph which are, of course, identical and parallel to each other. The shape of the patterns obviously depends on the orientation of the grain, affording a straightforward method of determining the local orientation of a grain, even when it is very small (see Fig. 8) [8, 20].

The channellographic method has been used to observe and measure the dechannelling due to the defects which have been theoretically studied and considered in Section 1.1. To this end, the same sample, both with and without defects , is bombarded with the same number of particles. Denoting the number of emerging particles for the two cases as N_d and N_o, respectively, the dechannelling cross-section σ_i of a defect i is given by

$$\tau = N_d/N_o = \exp - \int_0^t (\Sigma c_i \sigma_i)\, dz, \qquad (1)$$

where τ is the transmission coefficient, t is the thickness of the sample and c_i is the volumetric concentration of the defect i. This implies that the dechannelling due to a defect is not influenced by the presence of the other defects. For a sample containing only one kind of defect, but described by a distribution of sizes, we can replace $\Sigma\sigma_i c_i$, by $\bar{\sigma}c$, where $\bar{\sigma}$ is the mean value of the dechannelling cross-section of the "average" defect of total concentration c. Moreover, performing the "with-defects" and "without-defects" experiments at the same temperature eliminates the dechannelling contribution due to thermal agitation.

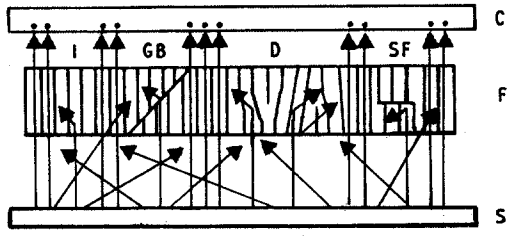

Figure 5 Schematic diagram of the channellographic method. The particles emitted by the source, S (α-particles or fission fragments), reach the crystal C. Their energy is adjusted in such a manner that only channelled particles can emerge from the crystal, on condition that they are not dechannelled by such as interstitials, I, grain boundaries, GB, dislocations, D and stacking faults, SF.

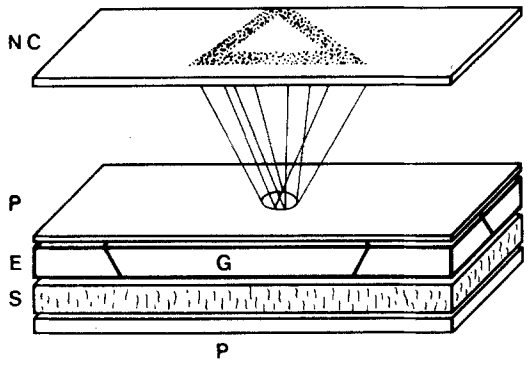

Figure 6 Schematic diagram of the channellographic projection method. The arrangement is similar to that presented in Fig. 5, but a small diaphragm, *P*, is put in front of a single crystal and the detector is removed to a greater distance. The channelled particles emerging from the sample describe on the detector a pattern whose geometrical shape depends on the structure and the orientation of the crystal.

1.2.1. Interstitial atoms

The experiment [21–23] consists of measuring the transmission of particles through thin samples in which foreign atoms have been introduced by thermal diffusion; this method avoids the formation of other defects such as dislocations that appear when ion implantation is used. As can be seen from Fig. 9, the transmission coefficient, τ, as a function of the interstitial concentration c (measured by resistivity) confirms the validity of Equation 1. In the case of hydrogen and carbon interstitials in palladium, we obtain $\sigma_H = (5.7 \pm 2.6) \times 10^{-5}$ nm^2 and $\sigma_C = (4.6 \pm 0.1) \times 10^{-5}$ nm^2 for H and C, respectively, in good agreement with the theoretical values given in Section 1.1.1. This shows that H and C interstitials do not appreciably deform the lattice, but the method does not permit the determination of the type of intersitial site (tetrahedral or octahedral) occupied, because both sites are located between {1 1 1} planes. This ambiguity is removed by direct site-location determination, as shown in Section 2 for the case of hydrogen interstitials.

1.2.2. Stacking faults

When a gold sample is quenched from high temperature ($T \geqslant 900°$ C) and then annealed at low temperature ($T \sim 100°$ C), vacancies precipitate and give rise to either Frank loops or stacking-fault tetrahedra. The dechannelling coefficient of a stacking-fault is measured by counting the number of particle tracks (see Fig. 10) that constitute the geometry of the patterns obtained by the channelling projection method, and by determining the concentration of stacking faults by electron microscopy. The experimental dechannelling coefficient thus obtained is $\chi \sim 0.17$, in good agreement with the theoretical value ($\chi_{\text{theoretical}} =$

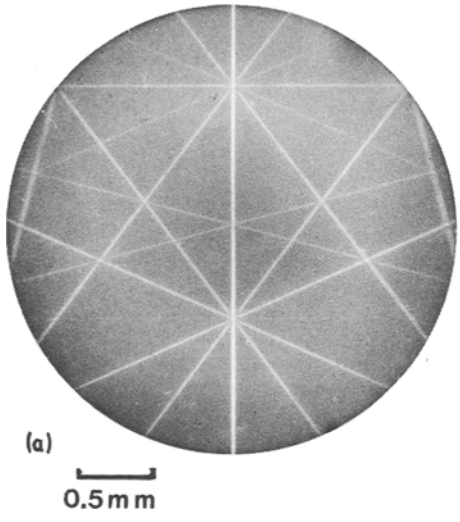

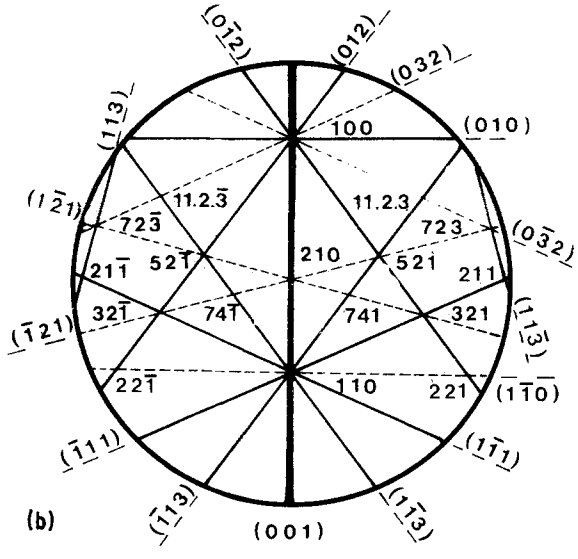

Figure 7 (a) Pattern obtained with a gallium crystal by means of the channellographic projection method, and (b) the corresponding indexing chart (temperature = 4 K) [18].

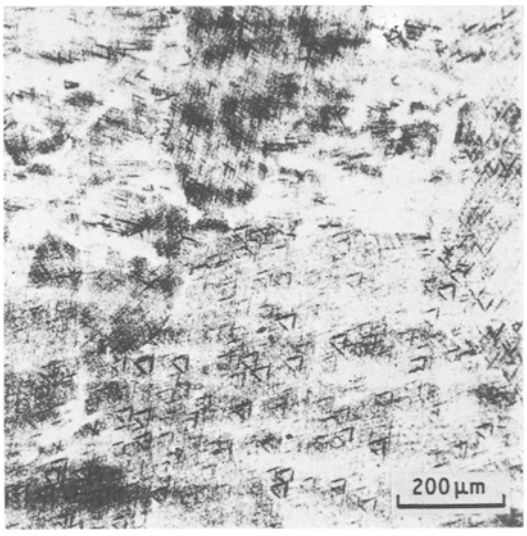

Figure 8 Channellograph of silver obtained with a radioactive source containing small-thickness inhomogeneties.

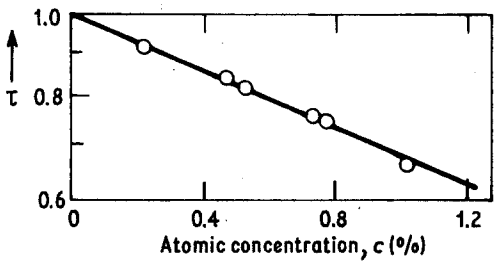

Figure 9 Variation of the transmission coefficient, τ, as a function of the atomic concentration, c, of dissolved carbon in palladium.

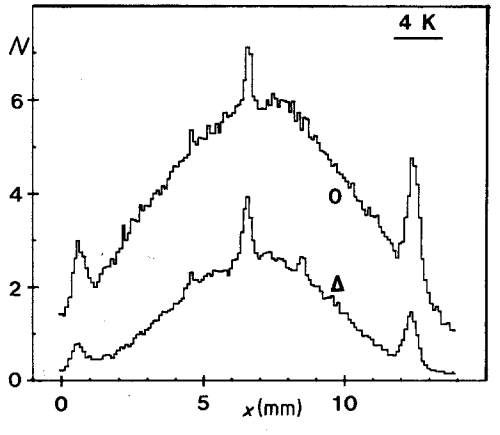

Figure 10 Influence of stacking faults on channelling in a gold sample. The channellographic projection is used, the patterns are triangles. The curves correspond to a sample either containing (Δ) or not containing (0) stacking faults. The experiment was conducted at 4 K.

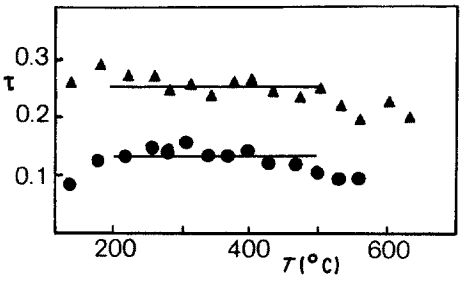

Figure 11 Transmission coefficient, τ, of an aluminium sample containing helium bubbles, measured at 300 K, as a function of the annealing temperature, T. Although the mean surface of the bubbles is multiplied by a factor of $\simeq 5$, τ varies only a little over the range of T from 473 to 773 K.

0.18) obtained in Section 1.1.2. In fact, the first experimental evidence of dechannelling by defects was obtained on stacking faults [24].

1.2.3. Gas bubbles

Helium gas is introduced into aluminium foils by irradiating them between two sheets of LiOH in a nuclear reactor. The number, n, and the radius, r, of the bubbles thus formed are measured after anneals by means of electron microscopy. According to previous studies [7, 25, 26], n decreases and r increases as the temperature increases. However, because of the high pressure, P, of the bubble ($P \sim 3500$ bars), the gas cannot be considered as perfect and the total projected surface $S = n\pi r^2$ of the bubbles is not constant. A complete calculation shows that, at least in the case of the small bubbles present in the samples studied here, the product of S and the dechannelling probability, χ, (see Section 1.1.5.) varies only slightly as a function of the radius of the bubble. This is clearly indicated in Fig. 11, which shows that, for a given total irradiation dose, the transmission coefficient is independent of the annealing temperature.

1.2.4. Dislocations and dislocation loops

The influence of dislocations [8–11, 27–31] is visible in Fig. 12 where both dechannelling in a region containing many dislocations and the very beginning of the thermal reordering of the crystal after a short anneal are observed. The dechannelling width, λ, of dislocations and dislocation loops were measured in aluminium. The values obtained, that is, $\lambda = (14 \pm 4)$ nm for straight dislocations and $\lambda = (0.5 \pm 0.3)$ nm for dislocation loops whose

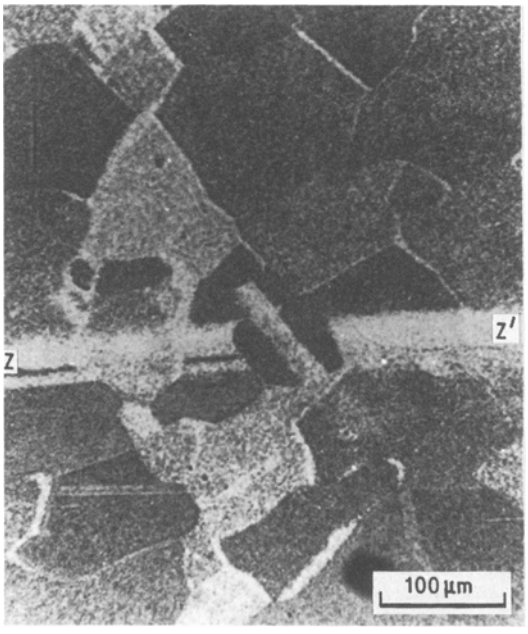

Figure 12 Example of dechannelling by dislocations. A polycrystal of nickel has been gently cold-worked along ZZ' and then slightly annealed at 1313 K. Particles are dechannelled along ZZ', but the beginning of recrystallization is visible in the middle of the channellograph. The particles used were protons, taken from a Van de Graaff accelerator [29]. This image also shows contrasts due to the different orientations of grains and twins, and the strong dechannelling effect of the grain boundaries (see also [33]).

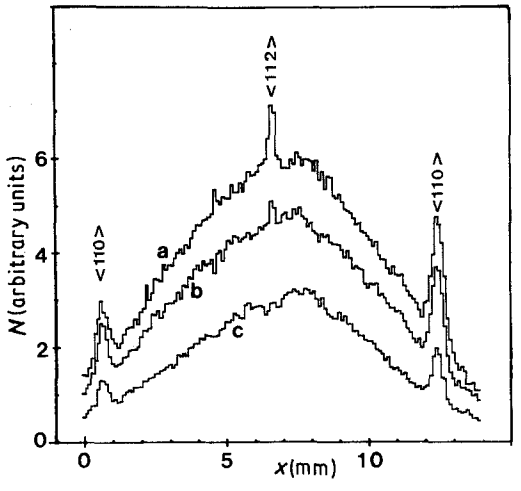

Figure 14 Influence of thermal agitation on channelling in gold. The sample is the defect-free sample used for the study of dechannelling by stacking faults (see Fig. 10). The experiments are carried out at (a) 4 K, (b) 77 K and (c) 300 K. Local peaks due to axial channelling (⟨100⟩, for instance) are clearly visible.

diameter is $d = 24$ nm, confirm the great difference between the two types of dislocations. In conjunction with results obtained in other laboratories [32, 34], the present results suggest a semi-empirical law relating λ to the diameter of the dislocation:

$$\lambda(d) = \lambda_\infty \frac{d}{d + d_o} , \qquad (2)$$

where λ_∞ is the value of λ for a straight dislocation, d is the diameter of the dislocation loop and d_o is an adjustable parameter (of the order of 500 nm). Moreover, isothermal annealing experiments have allowed us to measure the enthalpy, ΔH, of evaporation of dislocation loops in aluminium ($\Delta H = 1.32 \pm 0.1$ eV) and the enthalpy of recrystallization of platinum ($\Delta H = 2.6 \pm 0.2$ eV atom^{-1}), both results being in good agreement with the values obtained by other methods.

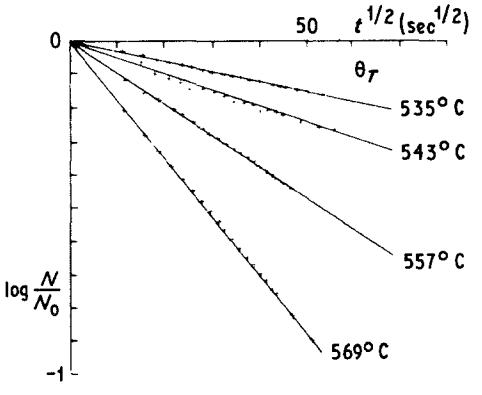

Figure 13 Variation of the transmission coefficient due to the clustering of Guinier–Preston zones in a Al–Cu alloy. N_o is the number of channelled particles just after the quench and N is this number of channelled particles after an ageing time, t, at 305 K; the quenching temperatures θ_T are indicated on each curve.

1.2.5. Guinier–Preston zones

Guinier–Preston (GP) zones have been studied in Al–Cu alloys quenched from different temperatures and aged at 32° C [7, 35, 36]. Fig. 13 shows the initial evolution of the transmission coefficient measured here by means of a scintillation counter, as a function of the ageing time, t. The dechan-

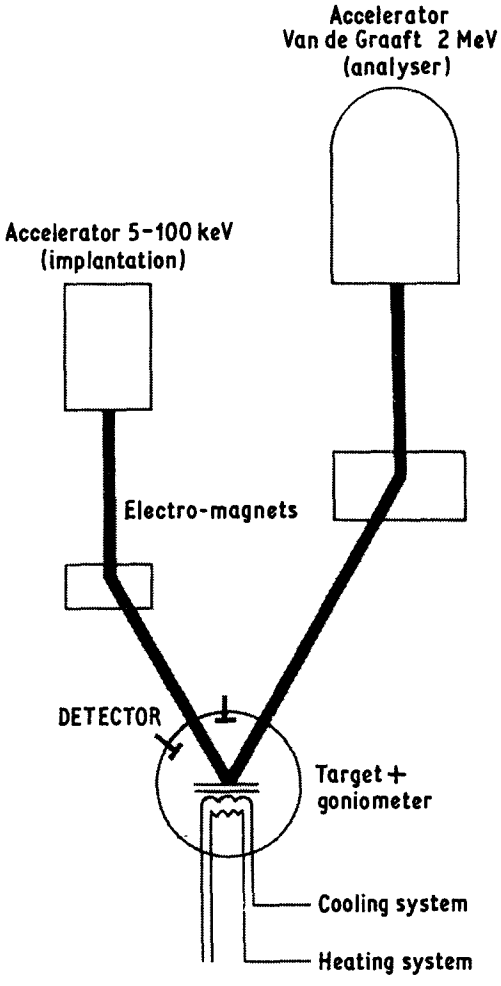

Figure 15 Experimental set-up used for lattice location. The sample is held on a goniometer, and hydrogen or deuterium ions are implanted in it by means of a low-energy accelerator. Profile drawings and lattice locations are obtained by means of a Van de Graaff accelerator.

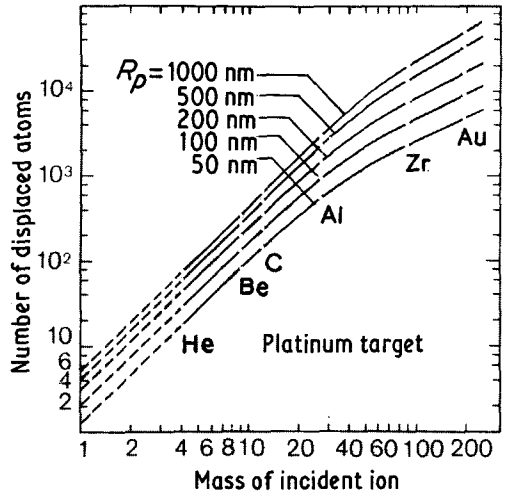

Figure 16 Variation of the number of displaced atoms in platinum by an ion implanted at various depths, R_p, as a function of the incident ion mass.

1.2.6. Ordered alloys

Experiments concerning dechannelling in ordered–disordered alloys are somewhat complicated owing to the difficulty in obtaining monocrystalline, or large-grain, thin foils. The method [13] consists of successively counting on channellographs all the

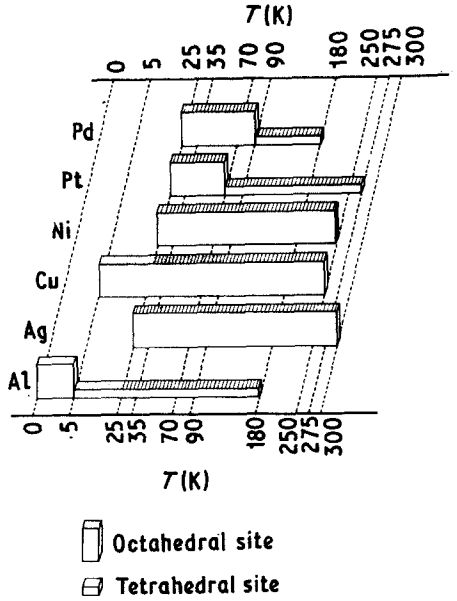

Figure 17 Lattice sites occupied by hydrogen in f c c as a function of the temperature: hatched areas indicate channelling results; stippled areas indicate muon results after [52, 53].

nelling increases very rapidly with time, and is very significant. As the dechannelling is adequately described by an exponential dependence on the square-root of t, it is concluded that the formation of the GP zones is due to fluctuations in the copper concentration (spinodal decomposition) rather than to nucleation followed by growth. Regarding a GP zones as a pseudo-dislocation loop, a dechannelling width, $\lambda = (4.5 \pm 2.5) \times 10^{-3}$ nm is measured when its diameter $d = 5$ nm. Finally, at long ageing times, the transmission curves tend toward the same value, that is, the final state of the alloy is the same, independent of quenching temperature.

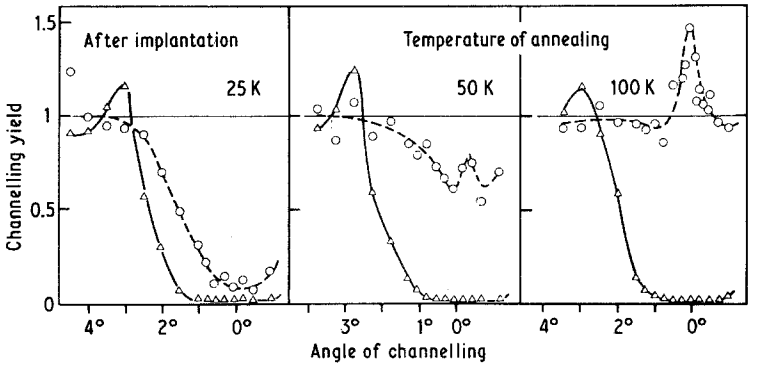

Figure 18 Channelling yield obtained along the ⟨100⟩-axis for platinum implanted with 10^{15} atoms cm^{-2} of 15 keV deuterium ions. The solid lines represent the interaction yields of ^3He ions with the platinum atoms located inside the rows limiting the channel as as a function of the angle of channelling, θ. The broken lines represent the interaction yield of ^3He ions with deuterium atoms as a function of θ. It can be seen that deuterium, initially in an octahedral site (at 25 K), migrates toward a nearly tetrahedral site after an anneal at about 50 to 100 K.

channelled particles associated with the ordered and disordered states of the same polycrystalline sample. It is thus observed that the transmission is much lower in the ordered state than in the disordered state (differences of up to 50% are observed), in accordance with the qualitative theory previously presented (see Section 1.1.6).

1.2.7. Thermal agitation

The channelling projection method is extremely convenient in demonstrating the effect of thermal agitation on channelling [3]. Counting the channelled particles emerging from a defect-free sample at different temperatures gives the curves appearing in Fig. 14. The number of channelled particles increases as the temperature decreases (compare with Section 1.1.7.). It is possible to determine a half-length of dechannelling (that is the distance $\lambda_{1/2}$ at which the number of channelled particles is reduced by a factor of 2 along their path in the crystal) due to both multiple scattering and thermal agitation. In gold, $\lambda_{1/2} = (1.33 \pm 0.05)\ \mu m$ and $(1 \pm 0.05)\ \mu m$ at 4 K and 300 K, respectively.

1.2.8. Composite dechannelling

Composite dechannelling [37, 38] is obviously an important case, generally encountered when a crystal is irradiated, and therefore contains different kinds of defects, such as interstitials, dislocations and dislocation loops.

It has been studied in many laboratories (see for example [39–42]), and our work consisted essentially of a study of the defects created by low-temperature (20 K) fission-fragment irradiations in iron samples containing carbon impurities. The channellographic method allowed demonstration of the large changes in cementite precipitation, a recovery stage of the dislocation loops starting from 800 K with an activation energy of about 1 eV, and the preponderant effect of clustering during certain stages of recovery.

2. Lattice location of hydrogen in face-centred cubic metals.

Shortly after the discovery of channelling, it was suggested that it could be used to locate foreign atoms in crystals both in interstitial and in substitutional sites [43, 44].

Such atoms to some degree obstruct certain channels and it is theoretically possible to locate them within an accuracy of about 0.02 nm.

One case in which the location of the lattice site is both important and difficult to determine by other methods (such as nuclear magnetic resonance, neutron diffraction) is that of hydrogen in face-centred cubic crystals (fcc), in which the solubility of hydrogen is generally very low.

In addition to being of fundamental interest, the determination of lattice location finds interesting application in the study of solid solutions obtained by implantation in materials either submitted to solar flare (space physics) or maintained in the presence of a plasma (controlled fusion).

Results are presented here for a series of fcc metals in which hydrogen has been implanted [45–51]. The maximum concentrations in the implanted layers range from about 10^{-4} to about 10^{-2} at.

2.1. Experimental set-up

The experimental set-up is represented in Fig. 15. The sample is held on a goniometer and maintained at a temperature that can be varied from 25 to 400 K during implantation and subsequent analysis.

To study these solutions, it is necessary to determine the lattice location and the concentration profile of hydrogen (or one of its isotopes) as a function of implantation and/or annealing temperatures.

To determine the lattice site occupied by a hydrogen (or isotope) atom, deuterium is implanted and is then located by means of a helium-3 beam using the non-resonant nuclear reaction $D(^3He, p)\alpha$. To study the profile, hydrogen is implanted and the analysis is made by means of a boron-11 beam through the resonant nuclear reaction $H(^{11}B, \alpha)\alpha\alpha$.

The implantation of hydrogen also induces defects such as vacancies and self-interstitials. The number of atoms displaced by ion implantation has been calculated in platinum and, by extrapolating the curves obtained to an ion of mass 1, it appears that this number is always greater than unity (see Fig. 16). It follows that, after implantation, a hydrogen (or deuterium) atom is always in the vicinity of some vacancies and interstitials. To distinguish hydrogen–crystalline-lattice interactions from hydrogen–defect interactions, the implantation is made at a temperature low enough ($T < 25$ K) to "freeze" interstitials, vacancies and hydrogen atoms in the lattice. Channelling is then used to locate hydrogen in this low-temperature "frozen" state and also to follow the evolution of its position with subsequent annealing steps. Alternatively, implantation can be performed at higher temperatures. Increased temperature renders the hydrogen and the defects mobile and during implantation higher temperatures can affect the number and nature of the defects.

2.2. Results

Hydrogen location has been studied in the following fcc crystals: Al, Ag, Ni, Cu, Pt and Pd. The results of the experiments are presented in Fig. 17, and the channelling curves allowing the location of hydrogen in platinum is given as an example in Fig. 18. As shown in Fig. 17, at 25 K (the low-temperature limit in our experimental conditions), hydrogen occupies an octahedral site in fcc metals, except for aluminium in which a tetrahedral site is found. However, other experiments made by implantation of muons strongly suggest that the octahedral position also exists in aluminium, but at a temperature much lower than 25 K [52, 53]. It can thus be concluded that, in general, at sufficiently low temperatures, hydrogen occupies an octahedral position in fcc metals.

With increased implantation or annealing temperatures, hydrogen atoms can move and, after a number of random jumps, they become trapped by defects. Two situations can be encountered.

Firstly, trapping can be accompanied by a site change. A transition is then observed from an initial octahedral site to a quasi-tetrahedral one in a trapped position. In Fig. 17, relating to platinum, it can be seen that hydrogen moves from the octahedral position to the tetrahedral one at about 50 K. This site transition due to trapping has also been observed for palladium and probably exists for aluminium.

Secondly, trapping is not accompanied by a change in the initial octahedral position (or only a very small change is seen, < 0.01 nm). This is the case for copper, nickel and silver. Here, the channelling technique does not allow a distinction to be made between the trapped and untrapped positions.

All our experiments confirm the conclusion that vacancies created during the implantation form traps for hydrogen. It is important to notice that, contrary to some theoretical predictions, we have never observed a substitutional position for hydrogen, in spite of the high concentration of vacancies during the implantation. Following our experimental results, new calculations have been performed by various authors that have shown that the existence of an equilibrium state located out of the centre of the vacancy is possible, which gives rise in particular to a tetrahedral site in aluminium.

Finally, it can be emphasized that, at high temperature, hydrogen leaves its trap to migrate over long distances in the crystal. It is interesting to notice that the tendency to agglomerate and form hydrogen bubbles has never been observed in these experiments on the fcc metals.

Acknowledgements

We are much indebted to Y. Quéré and H. M. Gilder for fruitful discussions and careful reading of the manuscript.

References

1. J. LINDHARD, *Mat. Fys. Medd.* **34** (1965) 1.

2. J. C. JOUSSET, J. MORY and J. J. QUILLICO , *J. de Phys.* **35** (1974) L 229.
3. J. MORY, CEA Report number CEA-R-4745 (1976).
4. Z. CHYLINSKI and A. DUNLOP, unpublished work (1981).
5. J. MORY, *J. de Phys.* **32** (1971) 41.
6. J. MORY and Y. QUÉRÉ, *Rad. Effects* **13** (1972) 57.
7. G. DÉSARMOT, CEA Report number CEA-R-4795 (1976).
8. Y. QUÉRÉ, CEA Report number CEA-R-3606 (1968).
9. *Idem. Phys. Lett.* **26A** (1968) 11.
10. *Idem. Ann. de Phys.* 5 (1970) 105.
11. *Idem, Rad. Effects* 38 (1978) 131.
12. H. KUDO *J. Phys. Soc. Japan.* **40** (1976) 1645.
13. J. CHEVALLIER, unpublished work (1974).
14. Y. QUÉRÉ, *Phys. Rev. B* **11** (1975) 1818.
15. S. STEENSTRUP, *Rad. Effects* **37** (1978) 51.
16. A. P. PATHAK, *Phys. Rev. B* **13** (1976) 1.
17. P. K. BHATTACHARAYA, J. CHEVALLIER, E. UGGERHØJ, J. MORY and Y. QUÉRÉ, *Rad. Effects* **51** (1980) 127.
18. J. TAKAHASHI and J. MORY, *Compt. Rend. Acad. Sci. Paris,* **292** (1981) 1123.
19. G. DELSARTE, CEA Report number CEA-R-4027 (1970).
20. G. DELSARTE, G. DÉSARMOT and J. MORY, *Phys. Stat. Sol.* **5** (1971) 683.
21. J. J. QUILLICO, CEA Report number CEA-R-4532 (1976).
22. J. J. QUILLICO and J. C. JOUSSET, *Phys. Rev. B,* **11** (1975) 1791.
23. A. DUNLOP, N. LORENZELLI and J. C. JOUSSET, *Phys. Stat. Sol. (a)* **49** (1978) 643.
24. Y. QUÉRÉ, J. C. RESNEAU and J. MORY, *Compt. Rend. Acad. Sci. Paris.* **262** (1966) 1528.
25. D. RONIKIER–POLONSKY, CEA Note number CEA-N-1834 (1976).
26. D. RONIKIER–POLONSKY, G. DÉSARMOT, N. HOUSSEAU and Y. QUÉRÉ, *Rad. Effects.* **27** (1975) 81.
27. H. COUVE, CEA Report number CEA-R-3741 (1969).
28. Y. QUÉRÉ and H. COUVE, *J. Appl. Phys.* **39** (1968) 1197.
29. J. LETEURTRE, N. HOUSSEAU and Y. QUÉRÉ and Y. QUÉRÉ, *J. de Phys.* **32** (1971) 205.
30. Y. QUÉRÉ and E. UGGERHØJ, *Phil. Mag.* **34** (1976) 1197.
31. G. CHALANT, CEA Note number CEA-N-1902 (1976).
32. G. CHALANT and J. MORY, *J. de Phys. Lett.* **40** (1976) L-473.
33. J. MORY and G. DELSARTE, *Rad. Effects.* **1** (1969) 1.
34. S. T. PICRAUX, E. RIMINI, G. FOTI and S. U. CAMPISANO, *Phys. Rev. B.* **18** (1978) 5.
35. G. DÉSARMOT, *Phys. Lett.* **46A** (1973) 159.
36. G. DÉSARMOT and Y. QUÉRÉ *Acta Met.* **28** (1980) 1375.
37. N. LORENZELLI, CEA Note number CEA-N-2102 (1979).
38. N. LORENZELLI, J. C. JOUSSET, *J. Nucl. Mater.* **69-70** (1978) 761.
39 K. L. MERKLE, P. P. PRONKO, D. S. GEMMEL, R. C. MIKKELSON and J. R. WROBEL, *Phys. Rev. B* 8 (1973) 1002.
40. E. BØGH, *Proc. Roy. Soc.* A **311** (1969) 35.
41. M. J. HOLLIS, C. S. NEWTON and P. B. PRICE, *Phys. Lett.* A **44** (1973) 243.
42. C. COHEN, F. ABEL, M. BRUNEAU, L. THOME, H. BERNAS and J. CHAUMONT, *Phys. Rev. B* **20** (1979) 1780.
43. S. T. PICRAUX, "Ion Beam Surface Layer Analysis" Vol. 2, edited by O. Meyer, G. Linker and F. Kappeler (Plenum Press, New York, 1976) p. 527.
44. H. D. CARSTANJEN, *Phys. Stat. Sol.* **59** (1980) 11.
45. J. P. BUGEAT, A. C. CHAMI and E. LIGEON, *Phys. Lett.* **58A** (1976) 127.
46. A. C. CHAMI, Thése, Université de Grenoble (1977).
47. E. LIGEON, J. P. BUGEAT and A. C. CHAMI, *Nucl. Inst. Meth.* **149** (1978) 99.
48. A. C. CHAMI, J. P. BUGEAT and E. LIGEON, *Rad. Effects* **37** (1978) 73.
49. J. P. BUGEAT and E. LIGEON, *Phys. Lett.* **71A** (1979) 93.
50. J. P. BUGEAT, Thése, Université de Grenoble (1979)
51. E. LIGEON, J. P. BUGEAT, R. DANIELOU, J. FONTENILLE and A. GUIVARC'H, *J. Radioanal. Chem.* **55** (1980) 376.
52. K. DORENBURG, M. GALDISCH, D. HERLACH, W. MANSEL, H. METZ, H. ORTH, G. ZU PUTLITZ, A. SEEGER and M. WIGAND, *Z. Phys.* **B31** (1978) 165.
53. O. HARTMANN, E. KARLSSON, K. PERNESTÅL M. BORGHINI, T. O. NIINIKOSKI and L. O. NORLIN, *Phys. Lett.* **61A** (1977) 141.

Received 26 June
and accepted 7 July 1981